# Crystal Structure of Recombinant Pea Cytosolic Ascorbate Peroxidase†

William R. Patterson‡ and Thomas L. Poulos*,‡,§

*Departments of Physiology and Biophysics and of Molecular Biology and Biochemistry, University of California, Irvine, California 92717*

*Received November 11, 1994; Revised Manuscript Received January 10, 1995*⊗

ABSTRACT: The crystal structure of recombinant pea cytosolic ascorbate peroxidase has been refined to an $R = 0.19$ for data between 8.0 and 2.2 Å resolution and $|F| \geq 2\sigma(|F|)$. The refined model consists of four ascorbate peroxidase monomers consisting of 249 residues per monomer assembled into two homodimers, with one heme group per monomer. The ascorbate peroxidase model confirms that the pea cytosolic enzyme is a noncovalent homodimer held together by a series of ionic interactions arranged around the 2-fold noncrystallographic dimer axis. As expected from the high level of sequence identity (33%), the overall fold of the ascorbate peroxidase monomer closely resembles that of cytochrome *c* peroxidase. The average root mean square differences for 137 helical α-carbon atoms between the four ascorbate peroxidase monomers and cytochrome *c* peroxidase and for 249 topologically equivalent α-carbon atoms are 0.9 and 1.3 Å, respectively. The active site structures are also the same, including the hydrogen-bonding interactions between the proximal His ligand, a buried Asp residue, and a Trp residue, whose indole ring is parallel to and in contact with the proximal His ligand just under the heme ring. This proximal Trp residue is thought to be the site of free radical formation in cytochrome *c* peroxidase compound I and is also essential for enzyme activity. The corresponding Trp in ascorbate peroxidase, Trp179, occupies exactly the same position. The most interesting, and possibly functionally important, difference between the two peroxidases is the presence of a cation binding site in ascorbate peroxidase located ~8 Å from the α-carbon atom of Trp179.

Plant ascorbate peroxidases (EC 1.11.1.11) exist as two distinct heme enzymes in the cytosol and chloroplasts that scavenge hydrogen peroxide by preferentially oxidizing ascorbate. These isozymes were first detected in spinach chloroplasts (Asada, 1981) and were studied in more detail in tea leaf cytosol and chloroplasts (Chen & Asada, 1989). Both enzymes catalyze the following multistep reaction:

$$\mathrm{APX(Fe^{3+})R + H_2O_2 \rightarrow \underset{\text{compound I}}{APX(Fe^{4+}{=}O)R^{\bullet}} + H_2O}$$

$$\mathrm{APX(Fe^{4+}{=}O)R^{\bullet} + \text{ascorbate} \rightarrow \underset{\text{compound II}}{APX(Fe^{4+}{=}O)R} + \text{monodehydroascorbate}}$$

$$\mathrm{APX(Fe^{4+}{=}O)R + \text{ascorbate} \rightarrow APX(Fe^{3+})R + H_2O + \text{monodehydroascorbate}}$$

The enzyme first reacts with peroxide to give compound I, where the heme iron is oxidized to the oxyferryl ($Fe^{4+}{=}O$) species and an organic group, R, either the heme ring or an amino acid side chain, is oxidized to a free radical. Compound I is reduced back to the resting ferric ($Fe^{3+}$) state by two successive one-electron reactions with the substrate, which, in the case of APX,[1] is ascorbate.

Purification of chloroplast APX from tea leaves indicated that the enzyme is a 34 000 Da monomer that is labile in the absence of ascorbate (Chen & Asada, 1989). Purification of cytosolic APX remained elusive until the enzyme was purified from pea shoots as a 57 500 Da homodimer that is stable in the absence of ascorbate (Mittler & Zilinskas, 1991a). Following the purification of pea cytosolic APX, the first available APX cDNA was sequenced and unexpectedly showed 33% amino acid identity with yeast cytochrome *c* peroxidase (CCP) (Mittler & Zilinskas, 1991b).

The high level of sequence identity between CCP and APX is especially interesting since, for nearly 3 decades, CCP has been the paradigm for structure−function relationships in the plant, fungal, and bacterial superfamily of peroxidases, including biochemical, biophysical, molecular biology, and X-ray diffraction studies (Poulos & Fenna, 1994). The CCP protein engineering system, consisting of a recombinant expression/purification system (Fishel et al., 1987) and a high-resolution crystal structure (Finzel et al., 1984), has allowed for detailed biochemical and biophysical studies of the peroxidase chemistry and mechanism, as well as biological electron transfer between CCP and its reducing substrate, ferrocytochrome *c* (Poulos & Fenna, 1994). Nevertheless, CCP is limited as a general model for peroxidases primarily because CCP is specific for cytochrome *c* as a reducing substrate, while nearly all other well-studied peroxidases

† This work was supported by National Science Foundation Grant MCB 9405218. W.R.P. was partially supported by National Institutes of Health Predoctoral Training Grant GM07311.

* Author to whom correspondence should be addressed at the Department of Physiology and Biophysics: Fax, (714) 824-8540; E-mail, poulos@uci.edu.

‡ Department of Physiology and Biophysics.

§ Department of Molecular Biology and Biochemistry.

⊗ Abstract published in *Advance ACS Abstracts,* March 1, 1995.

[1] Abbreviations: APX, recombinant pea cytosolic ascorbate peroxidase unless otherwise noted; CCP, cytochrome *c* peroxidase; $|F_o|$, observed structure factor amplitude; $|F_c|$, calculated structure factor amplitude; $\alpha_c$, calculated phases from the model; MIR, multiple isomorphous replacement; SIR, single isomorphous replacement; MIR/AS, multiple isomorphous replacement with anomalous scattering; NCS, noncrystallographic symmetry; rms, root mean square; $CH_3HgCl$, methylmercury chloride; $((CH_3)_3Pb)CH_3CO_2$, trimethyllead acetate.

0006-2960/95/0434-4331$09.00/0 

Table 1: Summary of Diffraction Data and Phasing Statistics[a]

| parameter | data set | | | | |
|---|---|---|---|---|---|
| | native | native anomalous | $CH_3HgCCl$ 1 | $CH_3HgCl$ 2 | $((CH_3)Pb)CH_3CO_2$ |
| conditions | | | 1 mM (3 h), wash (12 h) | 10 mM DTT (4 h), 1 mM (10 h), wash (4 h) | 1 mM (17 h) |
| no. of crystals | 1 | 3 | 1 | 1 | 1 |
| total observations | 184416 | 143224 | 82451 | 132734 | 61573 |
| unique reflections | 73104 | 35232 | 38921 | 44615 | 31450 |
| resolution (Å) | 2.2 | 2.5 | 2.6 | 2.4 | 2.8 |
| completeness at $I > 2\sigma(I)$ (%) | 91 | 84 | 82 | 85 | 76 |
| $R_{symm}$[b] (%) | 7.3 | 5.9 | 8.4 | 8.6 | 9.1 |
| no. of sites | | | 5 | 5 | 3 |
| $R_{Cullis}$[c] | | | 0.61 | 0.64 | 0.66 |
| overall phase power[d] | | | 1.4 | 1.4 | 1.4 |

[a]The overall mean figure of merit (18−3.0 Å) = 0.52 for 15 563 phased reflections at $F_{obs} > 5\sigma(F)$. [b]$R_{symm} = (\sum_{hkl}\sum_i|I_i(hkl) - \langle I_i(hkl)\rangle|/\sum_{hkl}\sum_i I_i(hkl))100$. [c]$R_{Cullis} = [\sum_{hkl}||F_{PH} \pm F_P| - F_{H(calc)}|]/[\sum_{hkl}|F_{PH} \pm F_P|]$. [d]Phase Power = $[\sum_n|F_H|^2/\sum_n|E|^2]^{1/2}$, where $\sum_n|E|^2 = \sum_n\{|F_{PH}|(obs) - |F_{PH}|(calc)\}^2$.

oxidize small organic molecules. Hence, identification of the structural factors controlling substrate specificity has remained elusive. In addition, CCP is unusual in that the reaction product with peroxidases, compound I, contains a free radical centered on Trp191 (Sivaraja et al., 1989), while other peroxidases generally form porphyrin $\pi$ cation radicals (Dolphin, 1971). Therefore, a protein engineering system utilizing a peroxidase that more closely resembles the enzymes that oxidize small organic and inorganic molecules would be highly desirable for probing structure−function relationships in peroxidases.

Toward this goal, we have developed a recombinant expression/purification system in *Escherichia coli* for pea cytosolic ascorbate peroxidase (Patterson & Poulos, 1994). An additional reason for focusing on APX is that the sequence data clearly indicate that, like CCP, APX has Trp residues located in the proximal and distal heme pockets (Mittler & Zilinskas, 1991b; Welinder, 1992). Moreover, since the proximal Trp191 in CCP is essential for the oxidation of cytochrome *c* (Mauro et al., 1988), APX provides an alternative system for studying the possible role of Trp in electron transfer from small molecule reducing substrates. The question of substrate specificity also may be somewhat easier to address by comparing APX with CCP, since they share such similar active site sequences yet exhibit very different specificities. As a first step in comparing structure−function relationships between APX and other peroxidases, we report herein the crystal structure of APX.

## MATERIALS AND METHODS

*Data Collection.* Recombinant APX from *E. coli* was purified and crystallized according to Patterson and Poulos (1994). The monoclinic APX crystals belong to space group *C*2, with $a = 132.4$ Å, $b = 53.0$ Å, $c = 170.6$ Å, and $\beta = 107.1°$, and contain two APX dimers per asymmetric unit. Native and heavy-atom diffraction data sets were collected from single crystals at ambient temperature using a Siemen's X-1000 area detector and rotating anode equipped with focusing optics. The raw intensity data were reduced and scaled using XENGEN (Howard et al., 1987). A native data set, optimized for detection of the heme $Fe^{3+}$ anomalous dispersion signal, was collected at ambient temperature from three crystals at the University of California at San Diego (UCSD) using two Mark III area detectors and a Rigaku rotating anode. The native anomalous dispersion data collection strategy was performed according to published guidelines (Xuong et al., 1985), and the raw intensity data were processed with in-house software (Howard et al., 1985). A summary of data collection and heavy-atom refinement statistics is presented in Table 1.

*Heavy-Atom Derivatives.* Initial phases were determined from isomorphous replacement methods using three heavy-atom derivative data sets from two different reagents (Table 1). Four of the five sites of the $CH_3HgCl$ derivative 1 were identified from an isomorphous heavy-atom difference Patterson. Single isomorphous replacement (SIR) phases from the $CH_3HgCl$ derivative 1 were used in cross-difference Fourier transforms, which located five sites in the $CH_3HgCl$ derivative 2 and three sites in the $((CH_3)_3Pb)CH_3CO_2$ derivative. SIR phases from the $CH_3HgCl$ derivative 2 were used in a native Bijvoet difference Fourier transform (UCSD native data set) that showed four strong peaks, presumably due to the four heme $Fe^{3+}$ atoms present in the asymmetric unit (i.e., two dimers composed of four monomers, with one heme $Fe^{3+}$ atom per monomer). The fifth site in the $CH_3HgCl$ derivative 1 was located by cross-Fourier synthesis calculated with multiple isomorphous replacement (MIR) phases from the $CH_3HgCl$ derivative 2 and the $((CH_3)_3Pb)CH_3CO_2$ derivative. Difference Pattersons, cross-difference Fourier transforms, and native Bijvoet difference Fourier transforms were computed using the program XtalView (McRee, 1992).

*Multiple Isomorphous Replacement.* Heavy-atom refinement, MIR phases, MIR/native anomalous (MIR/AS) phases, and solvent leveling calculations were performed with the program PHASES (Furey & Swaminathan, 1990). The heavy-atom and heme $Fe^{3+}$ coordinates, occupancies, and isotropic temperature factors were refined with data to 3.0 Å and $F/\sigma > 5$. Electron density maps calculated to 3.0 Å resolution using MIR or MIR/AS phases clearly indicated the molecular boundaries of the four monomers of the asymmetric unit, which were further enhanced by applying solvent leveling techniques. The anomalous dispersion data did not significantly improve the observed electron density and were not used in future phase calculations. However, in each monomer, defined electron density for two helices and the heme group was observed, but the remaining density was not interpretable. Since four identical monomers were present in the asymmetric unit of the APX crystal form, we sought to improve the MIR phases by determining the noncrystallographic symmetry (NCS) of the four asymmetric

unit monomers and applying 4-fold NCS averaging as a constraint for the MIR-generated electron density.

*Determination of Noncrystallographic Symmetry.* Self-rotation functions [X-PLOR (1992) and MERLOT (1988)] using the native APX data sets with varying resolution shells and Patterson vector lengths did not produce a solution(s) above the noise level. We next estimated the NCS operations using the $CH_3HgCl$ and heme $Fe^{3+}$ coordinates as follows. Biochemical and cDNA data (Mittler & Zilinskas, 1991a,b) indicated that each APX monomer contains one heme group and one cysteine residue, and the functional enzyme is a noncovalent homodimer. On the basis of this information, we assumed that each of the four monomers was represented by a heme $Fe^{3+}$ atom and that four of the five $CH_3HgCl$ sites represented the single cysteine residue in the four monomers. When these coordinates were displayed on a graphics system using the program SETOR (Evans, 1993), an obvious pattern indicated the most probable arrangement of the monomers/dimers. We assumed proper 2-fold NCS relating the monomers in the same dimer (i.e., point group 2), but realized that the NCS relating the monomers from the two different dimers would most likely be improper. Therefore, to relate any monomer to the second, we employed the following procedure. For each dimer, we defined midpoint atoms that represent the midpoints of the lines that connect the two Fe atoms of a dimer and the two mercury sites of the same dimer. Each monomer then was represented by four points in space: one Fe atom, one mercury site, one atom placed between the two Fe atoms of a dimer, and one atom placed between the two mercury sites of a dimer. By using these methods, the NCS operations that superimposed the monomers relative to a reference monomer (designated monomer 1) were calculated using PDBFIT (McRee, 1992).

*MIR Phase Improvement.* To refine and apply the estimated NCS operators, a molecular mask was created from CCP using the program MAMA (G. J. Kleijwegt and T. A. Jones, BMC, Uppsala, Sweden, personal communication) after the CCP molecule was manually oriented in the monomer 1 MIR electron density. The CCP mask and the NCS operators then were refined against the MIR electron density of APX at 3.0 Å using the program IMP (G. J. Kleijwegt and T. A. Jones, BMC, Uppsala, Sweden, personal communication). The correlation coefficients of the refined three NCS operators (excluding the identity operator) that transform monomer 1 to monomers 2−4 were 0.182, 0.183, and 0.192, respectively. The refined NCS matrices were input to a modified version of the program SQUASH (Zhang, 1993; Cowtan & Main, 1993; modified by D. J. Schuller, personal communication) for phase recombination using the 3.0 Å MIR phases, solvent leveling, histogram matching, and NCS averaging. The output SQUASHed maps calculated to 3.0 Å were markedly improved with clear, helical secondary structure and interpretable side-chain density. The 3.0 Å SQUASHed map was used as the starting point for model building.

*Model Building and Refinement.* Comparisons of the amino acid sequences of CCP and APX indicated that CCP could provide a rough starting model if certain portions of the CCP sequence were removed. The deleted sections were the N-terminal residues 2−10, a $\beta$-sheet consisting of residues 210−230, and the C-terminal residues 278−294. The edited CCP coordinates, including CCP side chains, were oriented in the electron density corresponding to the Hg and $Fe^{3+}$ atoms in monomer 1. The refined NCS operators that place monomer 1 to monomers 2−4 were used to place the edited CCP molecule in the four monomer positions of the APX asymmetric unit. Rigid-body refinement was performed using the four edited CCP molecules as the input coordinates against the native data set (X-PLOR, 1992). The *R*-factor at the end of 50 cycles was 0.45 for data between 10.0 and 3.0 Å. On the basis of this encouraging result, the output coordinates of the CCP molecule in the monomer 1 position were edited to replace the CCP side chains with the corresponding APX side chains. The newly constructed monomer 1 APX model was manually fit to the observed SQUASHed/MIR electron density map using the program TOM/FRODO, Alberta/Caltech Version 2.7 (Jones, 1985; A. Chirino and M. Israel, personal communication), and eventually included APX residues 11−247 (237 out of 249 total residues). The monomer 1 model was copied to the 2, 3, and 4 positions using the NCS operators to provide the model for simulated annealing refinement against data from 10.0 to 3.0 Å (X-PLOR, 1992) starting at 3000 K and finishing at 300 K. The *R*-factor of the annealed model was 0.26, and $(|F_o| - |F_c|)\ \alpha_c$ difference maps showed clear positive density for N-terminal residues 2−10 and C-terminal residues 248−250, which were deleted from the input model. Manual fitting with $(2|F_o| - |F_c|)$ and $(|F_o| - |F_c|)\ \alpha_c$ maps, inclusion of all 249 residues, and simulated annealing refinement (3000−300 K) against the native data (10.0−2.5 Å) brought the *R*-factor to 0.24. From this stage, all four monomers were treated as independent molecules and allowed to refine without NCS constraints. A final round of simulated annealing against native data from 12.0 to 2.2 Å followed by isotropic temperature factor refinement yielded an *R*-factor of 0.22. $H_2O$ molecules then were added manually according to stereochemical constraints and observed $(|F_o| - |F_c|)\ \alpha_c$ electron density $\geq 3\sigma$. Additional rounds of model building/$H_2O$ addition and positional refinement (100 cycles) followed by isotropic *B*-factor refinement (X-PLOR, 1992) reduced the *R*-factor to 0.19 for data between 8.0 and 2.2 Å and $|F| \geq 2\sigma(|F|)$ (Table 2).

Table 2: Summary of Crystallographic Refinement

| resolution range and $\sigma$ level | total reflections | *R*-factor[a] |
|---|---|---|
| 8.0−2.2 Å<br>$\|F\| \geq 2\sigma(\|F\|)$ | 51 337 | 0.19 |
| 8.0−2.2 Å<br>no $\sigma$ cutoff | 55 410 | 0.21 |
| all data<br>18.0−2.2 Å<br>$\|F\| \geq 2\sigma(\|F\|)$ | 52 471 | 0.20 |
| all data<br>18.0−2.2 Å<br>no $\sigma$ cutoff | 56 549 | 0.21 |
| RMS deviation of bond distances (Å) | 0.007 | |
| RMS deviation of bond angles (deg) | 1.279 | |
| RMS coordinate error determined from Sigma plot (Å) | 0.25 | |
| RMS coordinate error determined from Luzzati plot (Å) | 0.20−0.25 | |

[a] $R = \sum_{hkl}||F_{obs}| - |F_{calc}||/\sum_{hkl}|F_{obs}|$.

During $H_2O$ addition and the subsequent refinement, four water molecules in identical locations in the respective four monomers had *B*-factors $<10.0$ Å$^2$, and these oxygen atoms were within 3.5 Å of seven main-chain and side-chain oxygen atoms. In addition, the oxygen atom in monomer 1 was

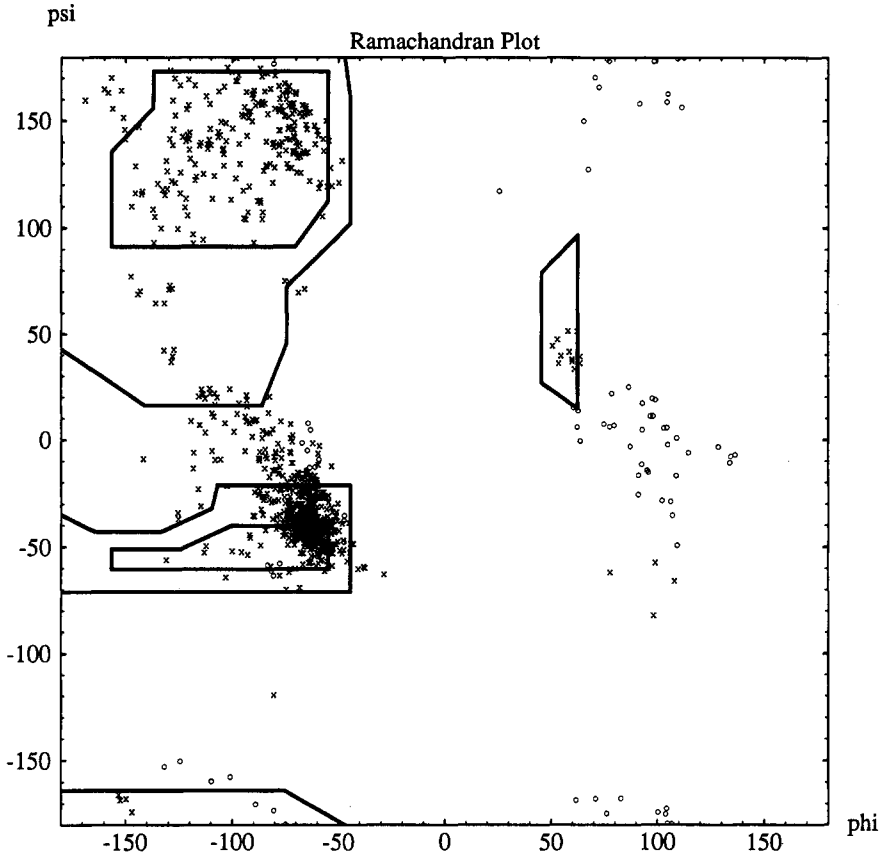


FIGURE 1: Ramachandran plot for the 996 residues in the APX asymmetric unit model. Glycines are represented by O. All other residues are denoted as ×.

observed in a 7$\sigma$ positive difference density peak, which indicated the presence of additional electrons. The positive difference density and the surrounding side-chain and main-chain oxygen atoms indicated that this site is occupied by a cation. The corresponding sites in monomers 2−4 were not associated with difference density contoured at ±3$\sigma$, suggesting either partial occupancy or substitution by a less electron-dense species. The average cation−ligand distance of 2.8 Å for the four APX monomer sites suggested $K^+$ (see Results). The four sites were modeled with $K^+$ scattering factors and were refined by two cycles of the following protocol: positional (25 cycles), *B*-factor (10 cycles group, 20 cycles individual), positional (25 cycles), and occupancy (25 cycles, only for the four cation sites) (X-PLOR, 1992). The occupancies of the $K^+$ ions in monomers 1−4 were 1.0, 0.63, 0.67, and 0.8, respectively. The *B*-factors for the $K^+$ ions in monomers 1−4 were 17.7, 14.2, 15.4, and 14.3 Å$^2$. Finally, APX crystals were grown in the presence of 150 mM potassium acetate, as opposed to the 150 mM sodium acetate we usually use, and a 90% complete data set to 2.7 Å ($I \geq 2\sigma(I)$) was collected (data not shown). Difference electron density maps indicated that the monomer 2−4 sites were now fully occupied with the cation, presumably $K^+$ (see Results). Cation−ligand distances were unrestrained during refinement, and electrostatic or van der Waals terms were not used.

Coordinate error analyses were performed with the Luzzati plot input file from X-PLOR (1992), with a Sigma script file from CCP4 (1994). rms deviations were calculated from superimpositions between CCP and APX with the program SUPERIMP (Honzatko, 1986) and between the monomers/dimers of the asymmetric unit with X-PLOR (1992).

## RESULTS

*Accuracy of the Model.* The APX asymmetric unit model includes 996 residues from two homodimers, dimer 1 and dimer 2, assembled from four monomers, designated 1−4, with 249 residues per monomer (dimer 1 = 1 + 2 and dimer 2 = 3 + 4). The N-terminal Met is not present in native APX (Mittler & Zilinskas, 1991a) and was removed in creating recombinant APX (Patterson & Poulos, 1994). Residue numbering, therefore, of the monomeric sequences begins with the second amino acid, Gly2, and ends with Ala250. Each monomer contains one molecule of ferric protoporphyrin IX heme and one cation (modeled as $K^+$, see the following), and the asymmetric unit model contains 649 solvent molecules. Twenty residues, located on the surfaces of the respective monomers, were disordered and did not have sufficient electron density for unique conformational assignments, and, additionally, the C-termini of the four monomers were disordered. Six residues were present in dual conformations, and no attempt was made to model the extra conformations.

As shown in Table 2 and Figure 1, the model exhibits excellent geometry. The Ramachandran diagram (Ramakrishnan & Ramachandran, 1965) of the APX model (Figure 1) shows most residues in allowed regions of α-helix with loop residues predominantly occupying the β-sheet region. Glycines are more diffusely positioned in the APX model, and 11 residues occupy the left-handed α-helix region of the Ramachandran plot. Left-handed helices were not observed in the structure, and these residue $\phi,\psi$ angles represent deviations. The overall rms deviations between Cα-atoms of the respective monomers and dimers in the asymmetric unit are ≤0.4 Å for the seven unique compari-

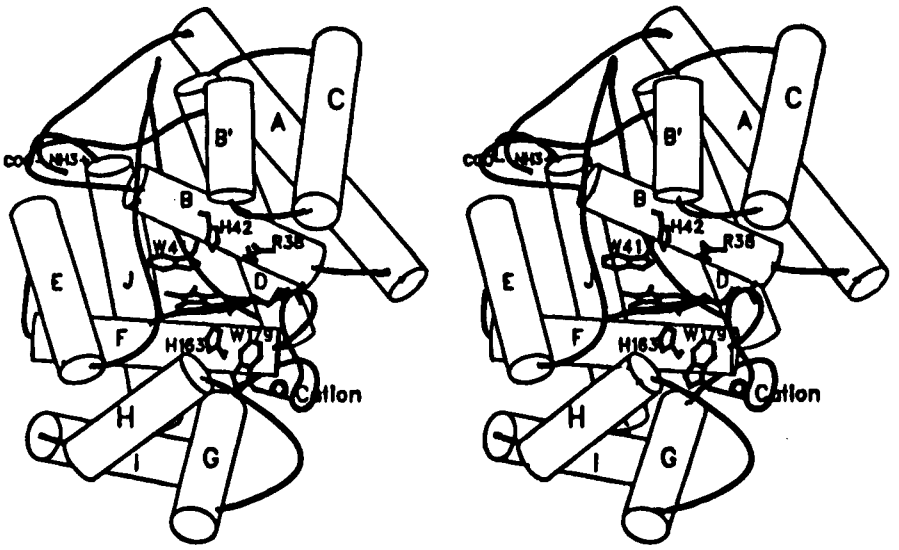


FIGURE 2: Schematic stereo representation of APX monomer 1. Helices are indicated by cylinders with nomenclature corresponding to Table 3. Relevant proximal and distal residue side chains are displayed near the heme group and labeled by residue name (one-letter code) and number. The proximal cation binding site is indicated by the label cation. Figures 2–9 were generated with the programs SETOR (Evans, 1993) or MOLSCRIPT (Kraulis, 1991).

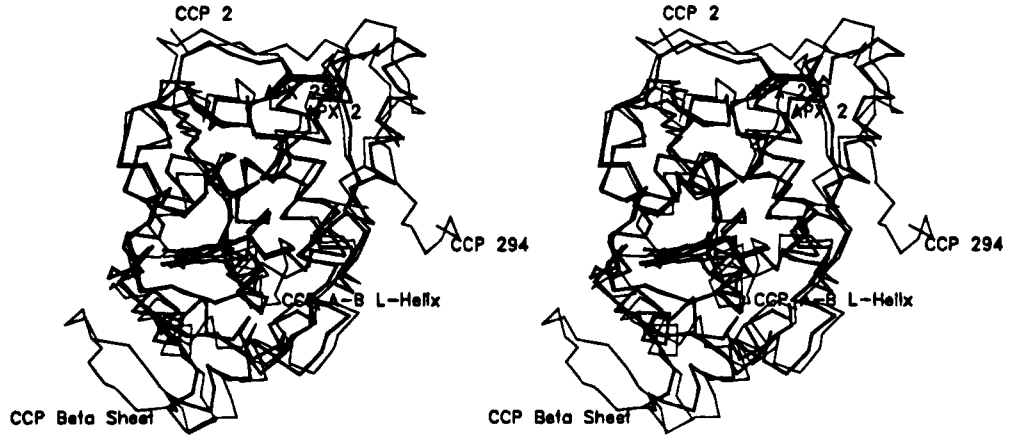


FIGURE 3: Stereo representation of the superimposition of CCP and APX monomer 1. APX is in bold lines. The N- and C-termini for CCP and APX are labeled CCP2/CCP294 and APX2/APX250, respectively. The $\beta$-sheet, present in CCP but absent from APX, is indicated by the label CCP Beta Sheet. The single turn of left-handed $\alpha$-helix present in CCP, between the A- and B-helices but absent from APX, is indicated by the label CCP A–B L-Helix.

sons. The rms deviations of C$\alpha$-atoms are 0.2–0.25 and 0.25 Å based on Luzzati plots (Luzzati, 1952) and Sigma analysis (Srinivasan, 1966), respectively.

*Comparison of the APX and CCP Structures.* For simplicity and in accordance with the 33% sequence identity between CCP and APX, the APX monomer will be compared to CCP as the representative member of class I intracellular peroxidases in the superfamily of plant, fungal, and bacterial peroxidases as defined in the literature (Welinder, 1992). A schematic diagram of APX is shown in Figure 2, and a superimposition of CCP on APX is shown in Figure 3. The domain structure of the monomer unit is nearly identical to CCP consisting of domain I (N- and C-termini, helices A–D) and domain II (helices F–J). The domains are connected via the E-helix. The J-helix, which begins in domain II, extends into domain I where the C-terminus ends within 4 Å of the N-terminus. The truncated APX C-terminus, relative to CCP, does not include the J′-helix of CCP.

As indicated in Table 3, the APX helices were designated according to the nomenclature of Finzel et al. (1984). Differing from CCP, helices A, B′, C, and D terminate with one turn of $3_{10}$-helical geometry. However, the F-helix of APX terminates with two full turns of $3_{10}$-helix analogous to the F-helix of CCP. The average rms difference for 137 C-$\alpha$-carbon atoms in a helical conformation is 0.9 Å, while that for 249 topologically equivalent C-$\alpha$-atoms is 1.3 Å. The average rms differences were calculated from the rms

Table 3: Helical Structure of APX[a]

| helix | beginning | end | no. of residues |
|---|---|---|---|
| A | P10 | K31[b] | 22 |
| B | A33 | A44 | 12 |
| B′ | Q63 | A67[b] | 5 |
| C | D75 | Q87[b] | 13 |
| D | Y93 | T108[b] | 16 |
| E | H140 | M149 | 10 |
| F | D153 | S160[c] | 8 |
| F' | H169 | G174 | 6 |
| G | S189 | T196 | 8 |
| H | P206 | L211 | 6 |
| I | S215 | A226 | 12 |
| J | E228 | S243 | 16 |

[a]Helices were defined by torsion angles and hydrogen-bonding pattern (distance 2.5–3.5 Å). Helical designation follows the CCP nomenclature in Finzel et al. (1984). [b]Indicates helices that are terminated by one turn of $3_{10}$-helical geometry. [c]Residues 161–165 form two full turns of $3_{10}$-helical geometry.

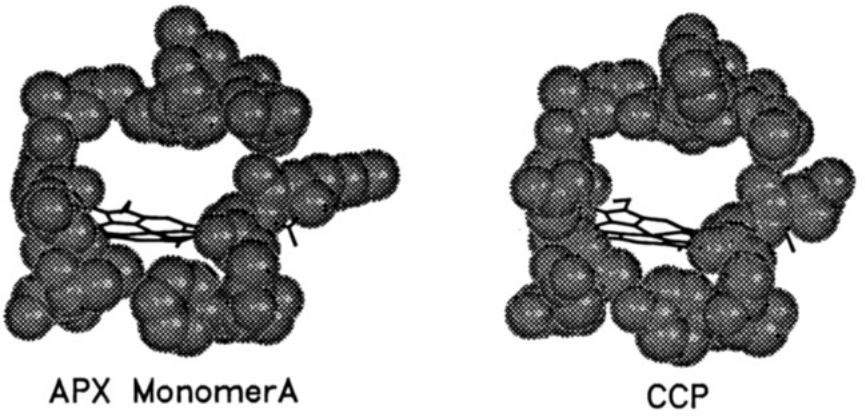


FIGURE 4: Comparative views of the distal heme exposure for the APX monomer and CCP.

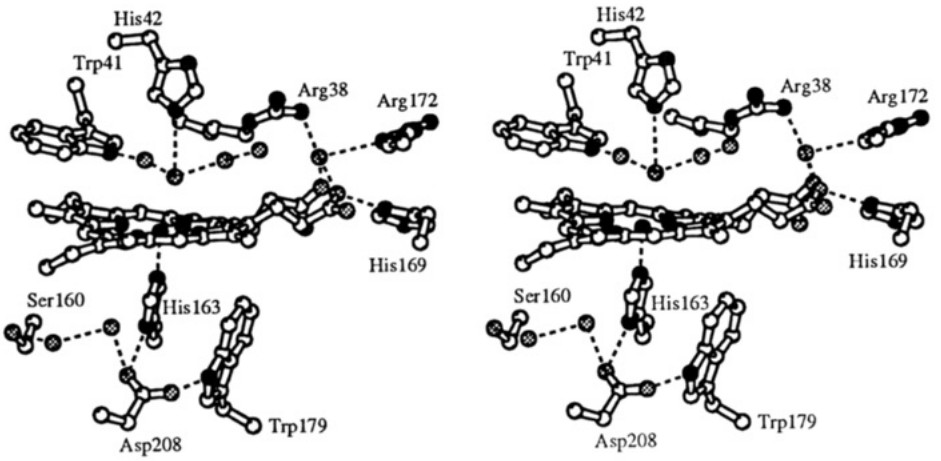


FIGURE 5: Stereo representation of the proximal and distal APX monomer active sites. Carbon atoms are open circles, nitrogen atoms and the heme Fe are black circles, and water oxygen atoms are gray circles. Dashed lines indicate H-bonds.

differences of the individual superimpositions for each of the four APX monomers onto CCP.

APX contains less $\beta$-structure than CCP. The residues that, in CCP, form two of the three strands in the CCP $\beta$-sheet are deleted from the APX sequence and from the APX structure. Residues 133−136 form a standard type I $\beta$-turn with an $i + 3$ hydrogen bond, while residues 48−53 form a $\beta$-bulge turn with an $i + 4$ hydrogen bond and a $\beta$-pair hydrogen bond between residues 48 and 53. Turns were classified according to terminology presented in Richardson and Richardson (1989).

The access channel connecting the molecular surface to the distal heme pocket is very much the same in size and shape in both peroxidases (Figure 4). The heme also is anchored in place by similar sets of interactions but with some interesting variations. For example, His169 (His181 in CCP) forms an H-bond with one of the heme propionates (Figure 5). In CCP, however, His181 also interacts with Asp37, which is part of an unusual left-handed helical turn. Asp37 is thought to be important for the recognition of cytochrome *c* (Pelletier & Kraut, 1992). This interaction is not present in APX since APX is missing the left-handed helical turn containing Asp37 found in CCP. One other difference is that, in CCP, Asn184 interacts with a heme propionate while the equivalent residue in APX is Arg172, which forms an H-bond with a water molecule that is hydrogen-bonded to both heme propionates and Arg 38 (Figure 5).

*APX Dimer Interface.* The dimer interface of the APX homodimer (Figure 6) is mediated primarily by electrostatic interactions between Asp, Glu, Arg, and Lys side chains. In Table 4 are the relevant residues and the distances of closest approach. The electrostatic contacts are arranged around the 2-fold NCS dimer axis, so that, for example, Lys18 in monomer 1 pairs with Asp229 in monomer 2, while Asp229 in monomer 1 pairs with Lys18 in monomer 2. Note that all of the salt bridge distances listed in Table 4 do not strictly conform to the preceding 2-fold criterion, which suggests imperfection in the dimeric NCS operation or that NCS contacts with the adjacent dimer influence the interactions (see Discussion).

*Active Site Structure.* The active site structures of CCP and APX are superimposed in Figure 7. As expected, the structures are very similar. The distal pocket of all APX monomers contain more than four ordered solvent molecules, which were removed from Figure 7 for clarity. The proximal side superimposition shows that the proximal ligand His163, the buried-charged residue Asp208, and Trp179 are in nearly identical conformations in the two peroxidases. Since special functional significance has been assigned to the His-Asp-Trp catalytic triad (Goodin & McRee, 1993), it is important to examine more closely the detailed interactions between these groups and the surrounding environment (Figure 5). The average hydrogen bond distance over the four monomers for the Asp208−His163 pair is 3.2 ± 0.1 Å and that for the Asp208−Trp179 pair is 2.8 + 0.1 Å. The corresponding distances are 3.0 and 2.8 Å in CCP. Hence, the His-Asp H-bond may be stronger in CCP than in APX. In addition, two $H_2O$ molecules in each of the four APX monomers are present near the Asp208−His163 hydrogen bond (Figure 5). One $H_2O$ molecule is 2.7 ± 0.1 Å from the O$\delta$1 of Asp208. This $H_2O$ molecule is also present in CCP (Finzel et al.,

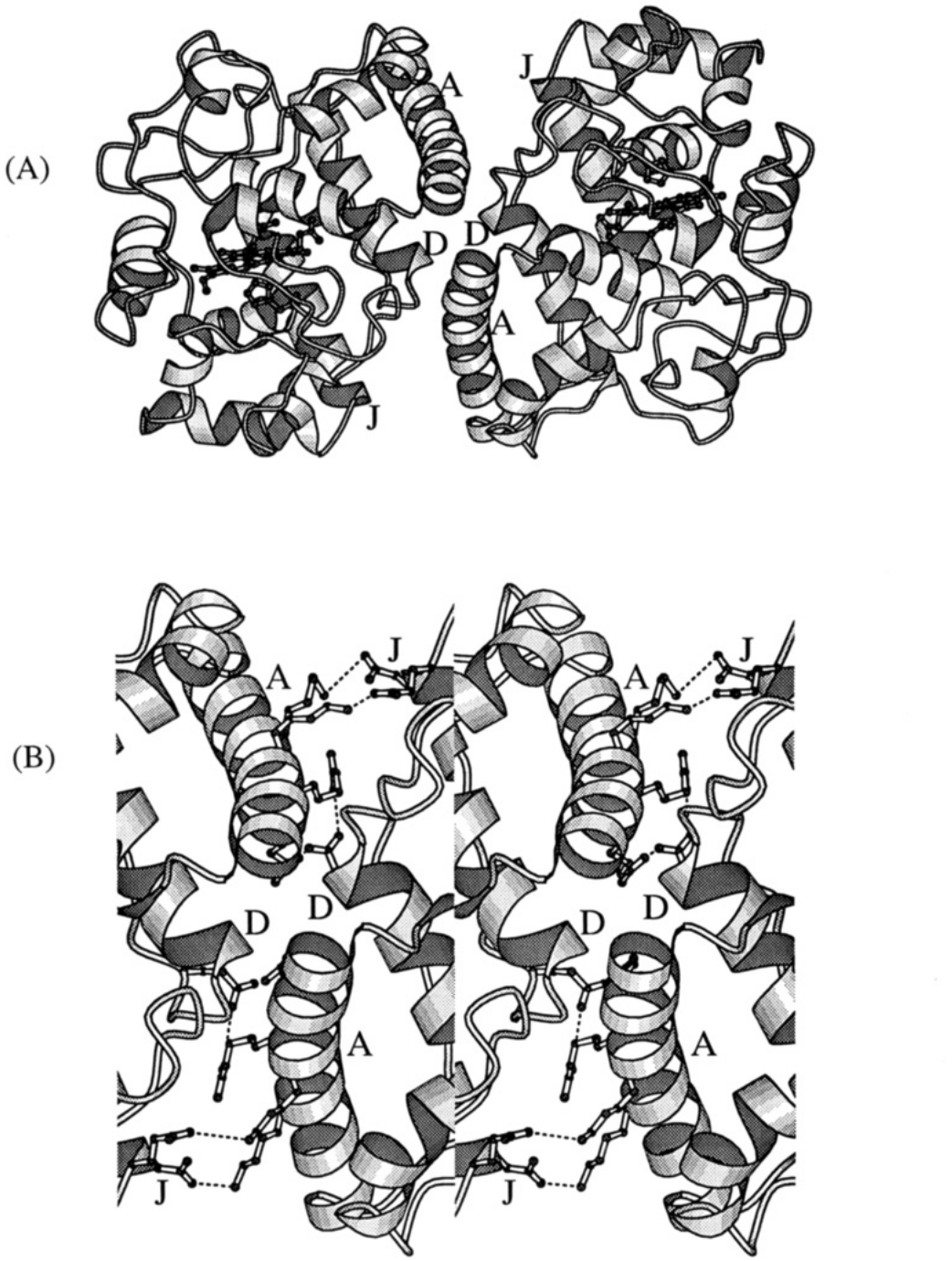


FIGURE 6: (A) Ribbon representation of APX dimer 1. The 2-fold, noncrystallographic dimer axis is perpendicular to the plane of the page, and helices A, D, and J are labeled. The proximal His163 side-chain is present in each monomer. (B) Magnified stereo diagram of the APX dimer 1 interface in the same orientation as in (A). Electostatic interactions are indicated by dashed lines.

1984). The second APX $H_2O$, which is 3.0 ± 0.4 Å from the first $H_2O$ and 4.1 ± 0.2 Å from Asp208 Oδ1, is not present in CCP. In CCP, Met172 is about 3.8 Å from the buried Asp, while the corresponding residue in APX is Ser160 (Figure 5). Hence, the electrostatic environment near the Asp-His pair differs significantly in the two peroxidases.

A potentially important and unexpected difference is the presence of a cation near the proximal catalytic triad of APX that is not present in CCP (Figure 8). A cation was assigned to this site on the basis of large positive difference electron density at 7$\sigma$, even when a water oxygen atom was modeled at this position in monomer 1 (Figure 8). The cation coordination sphere exhibits distorted pentagonal bipyramidal geometry with one Asp Oδ2 ligand, two Thr Oγ1 ligands, three carbonyl main-chain oxygen ligands, and no aqua ligands. The average distance (average of the four monomers) from the cation to the Cα of Trp179 was 7.6 ± 0.1 Å. Additionally, a water molecule was observed at an average distance of 5.2 ± 0.1 Å (average of the four monomers) from the cation and an average distance of 3.9 ± 0.2 Å from the Cε3 atom of Trp179 (Figure 9). The isotropic temperature factors for the four water molecule oxygen atoms found in this position were 2.0, 13.9, 16.1, and 16.3 $Å^2$ for monomers 1−4, respectively.

*Modeling the APX Cation Sites.* The assignment of $K^+$ is based on computational analysis, although the analysis gives nearly identical results with $Ca^{2+}$ (18 electrons) scattering factors in place of $K^+$ scattering factors (data not shown). Additionally, the cation binding sites in the four monomers are similar to the proximal $Ca^{2+}$ sites located in

Table 4: Amino Acid Residues Involved in APX Dimerization

| dimer 1 | | distance (Å) |
|---|---|---|
| monomer A | monomer b | (atom A to atom B) |
| K18 | D229 | 3.3 (Nζ to Oδ1)[a] |
| D229 | K18 | 3.4 (Oδ1 to Nζ) |
| R24 | E112 | 3.5 (NH1 to Oε1) |
| E112 | R24 | 2.8 (Oε1 to NH1) |
| R21 | E112 | 4.2 (NH2 to Oε2) |
| E112 | R21 | 3.1 (Oε2 to NH2) |
| K22 | E228 | 5.2 (Nζ to Oε2)[a] |
| E228 | K22 | 3.1 (Oε2 to Nζ) |
| **dimer 2** | | **distance (Å)** |
| monomer C | monomer D | (atom C to atom D) |
| K18 | D229 | 3.1 (Nζ to Oδ1) |
| D229 | K18 | 4.7 (Oδ1 to Nζ)[a] |
| R24 | E112 | 2.8 (NH1 to Oε1) |
| E112 | R24 | 2.8 (Oε1 to NH1) |
| R21 | E112 | 3.6 (NH2 to Oε2) |
| E112 | R21 | 3.8 (Oε2 to NH2) |
| K22 | E228 | 4.2 (Nζ to Oε2) |
| E228 | K22 | 4.7 (Oε2 to Nζ)[a] |

[a] Residues 18, 22, 228, and 229 in the indicated monomers are in the noncrystallographic contact regions of the A–D monomers.

fungal peroxidases (Poulos et al., 1993; Kunishima et al., 1994; Peterson et al., 1994; Sundaramoorthy et al., 1995). However, APX contains only one carboxylate group as a ligand, while in the fungal peroxidases, two carboxylates participate. Electroneutrality is often maintained in protein–metal binding sites by supplying the appropriate number of charged amino acid side chains, so that the net charge of the coordinating charged side chains cancels the ionic charge of the metal (Glusker, 1991). The presence of a single carboxylate in the APX cation site, therefore, suggests a monovalent cation. Moreover, the average cation-ligand distance in the four monomers is 2.8 Å (Table 5), which is in excellent agreement with the 2.7–2.8 Å metal–oxygen distances reported for $K^+$ and markedly different from the 2.4 Å metal–oxygen distances for $Na^+$ and $Ca^{2+}$ (Glusker, 1991).

The assignment of $K^+$ in monomers 2–4 with fractional occupancies is also influenced by the knowledge that the APX protein, which is stored in 50 mM potassium phosphate buffer (pH 7), is crystallized in 100 mM Tris Cl (pH 8.5), 22% PEG 4000, and 150 mM sodium acetate (Patterson & Poulos, 1994). The reason why monomer 1 exhibits such a large (i.e., 7σ) difference peak may be because, in the crystal structure, the monomer 1 cation site is less solvent-exposed than the other monomer sites. Therefore, partial $K^+$ occupancies in monomers 2–4 would explain the absence of positive difference density in these positions.

Toney et al. (1993) demonstrated dramatic changes in one of two cation sites in dialkylglycine decarboxylase, where the exchange of $Na^+$ for $K^+$ results in the reduction of the average metal–ligand distance from 2.7 to 2.3 Å. We did

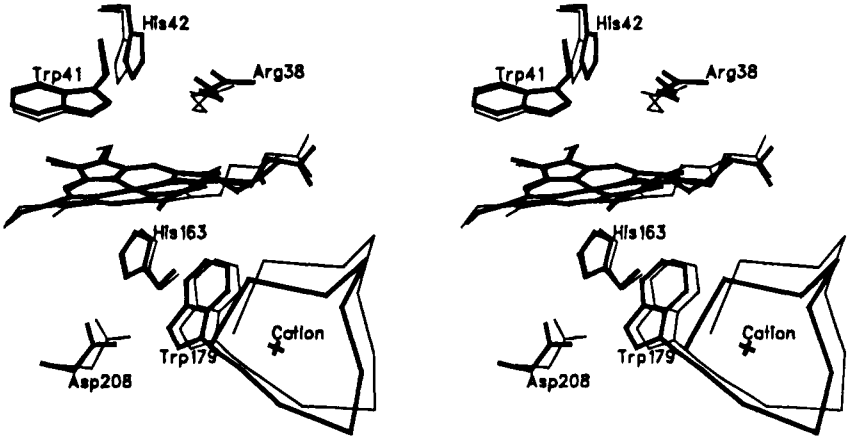


FIGURE 7: Stereo representation of the superimposition of CCP and the APX monomer. The relevant distal and proximal residue side chains, including the C α-atoms that form the proximal cation binding site in the APX monomer, are displayed for both molecules. APX is in bold lines. The label cation refers to the location of the cation binding site in the proximal APX monomer heme environment. APX residues are indicated by their respective residue name (three-letter code) and number.

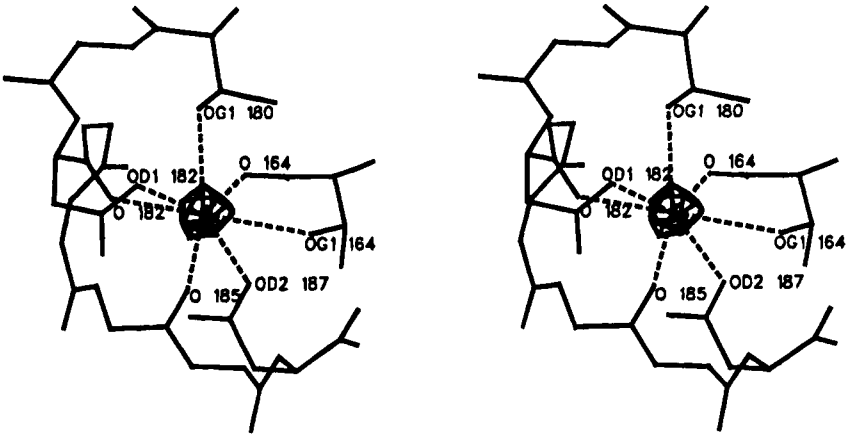


FIGURE 8: Stereo representation of the APX monomer 1 cation binding site. Coordinating side-chain atoms are labeled. The positive electron difference density (coefficient $(|F_o| - |F_c|)\exp(-(I\alpha_{calc}))$) was contoured at 7σ and results when an oxygen or $Na^+$ atom is modeled at the site.

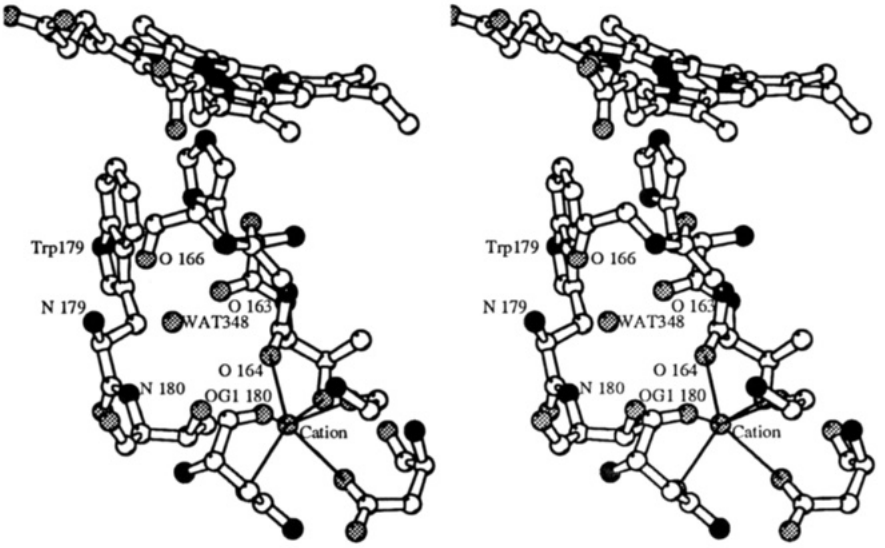


FIGURE 9: Stereo representation of the APX monomer 1 cation and nearby solvent molecule (WAT348). Oxygen atoms and the cation are gray, nitrogen atoms are black, and carbon atoms are white. Coordination bonds from the protein to the cation are denoted in solid, black lines.

Table 5: Average Cation−Ligand Distances ($n = 4$ Monomers) from the APX Cation Sites

| ligand | average distance (Å) |
|---|---|
| T164 (C′O) | 2.5 ± 0.1 |
| T164 (Oγ1) | 3.0 ± 0.2 |
| T180 (Oγ1) | 2.9 ± 0.1 |
| N182 (Oδ1) | 2.8 ± 0.2 |
| N182 (C′O) | 2.7 ± 0.1 |
| I185 (C′O) | 2.5 ± 0.1 |
| D187 (Oδ2) | 3.2 ± 0.2 |
| cumulative average ($n = 7$) | 2.8 ± 0.3 |

[a] Data are mean ± 1 standard deviation. C′O indicates carbonyl oxygen as the donating ligand

not observe significant differences in cation−ligand distances between monomer 1 and monomers 2−4, suggesting that $Na^+$ may be unable to fully replace $K^+$ in the cation site or that the backbone geometry of the site is quite rigid. Therefore, for the purposes of modeling the cation sites, we excluded $Na^+$ on the basis of metal−ligand distances and $Ca^{2+}$ on the basis of ligand distances and electroneutrality.

Finally, in order to test whether monomers 2−4 can bind $K^+$, crystals were grown using potassium acetate rather than sodium acetate (see Materials and Methods). Initial ($|F_o| - |F_c|$) $\alpha_c$ electron density maps at 2.7 Å show 4$\sigma$ peaks at monomer sites 2−4 when $Na^+$ is modeled at these sites, while the monomer 1 site does not show 4$\sigma$ positive difference density when modeled with $K^+$ (data not shown). These data, the metal−ligand distances, and the preference for maintenance of electrical neutrality strongly suggest that $K^+$ is the preferred cation in all four monomers.

## DISCUSSION

*Overall Structural Comparisons.* As shown in Figure 3, the helical topology of the APX monomer is nearly identical to that of CCP. In the past 2 years, three fungal peroxidase structures from the superfamily of plant, fungal, and bacterial peroxidases became available for comparison to CCP (Poulos et al., 1992; Sundaramoorthy et al., 1994; Kunishima et al., 1994; Peterson et al., 1994). By comparing these structures to CCP, it is apparent that, although the sequence identity is <20%, the tertiary structure is similar throughout the four structures. The crystal structure of APX continues the trend in this superfamily, demonstrating that tertiary structure is highly conserved. Differences do occur in the N- and C-termini where these regions are truncated relative to CCP, and the N-terminal difference causes a shift in the A-helical axis of APX relative to the CCP A-helix. The N-termini may, in fact, be electrostatically paired to the respective C-termini at physiological pH. Crystals of APX were formed at pH 8.5 where the N-terminal amino group is largely deprotonated ($\sim pK_a = 7.5$). Although the C-termini were disordered in the monomers, electron density was available to roughly fit the carboxylate group and estimate the distance from C-terminus to N-terminus as ~3 Å. The C-terminal disorder, then, may be due to the increase in pH preventing electrostatic interaction of the termini. Two loops, present in CCP, are not present in the APX monomer structure. First, the loop that forms the $\beta$-sheet in domain II of CCP is completely omitted in APX, which was anticipated by sequence alignment between CCP and APX (Welinder, 1992). Second, a connecting turn of left-handed helix between the A- and B-helices in domain I of CCP is absent from the APX monomer (Figure 3).

The most notable difference between CCP and APX is the presence of quaternary structure in APX (Figure 6). Gel filtration chromatography demonstrated that native APX is a noncovalent homodimer of $M_r$ 57 500 (Mittler & Zilinskas, 1991a). The literature on ascorbate peroxidases purified from different plant species and tissues, such as tea leaves, maize seedlings and leaves, and potato tubers, reports the isolation of both monomeric and dimeric forms (Chen & Asada, 1989; Koshiba, 1993; Elia et al., 1992). The APX crystal structure shows specific electrostatic contacts in the region of the dimer interfaces (Figure 6). As many as eight salt bridges, arranged around the NCS dimer 2-fold symmetry axis, may stabilize the dimeric form of APX. In the asymmetric unit of the APX crystals, four of the salt bridge residue pairs are within the NCS contact regions of the two dimers, and three of these pairs exhibit distances >4.5 Å in one dimer, but are <4 Å in the other dimer. This result indicates that the salt bridges do not conform perfectly to the 2-fold dimer symmetry or that the dimer/dimer NCS contacts may be influencing the salt bridge distances. In either case, dimer 1 contains six

and dimer 2 contains five salt bridges with distances <4 Å. The dimer interfaces contain ordered solvent molecules, although defined hydrogen bond interactions were not apparent.

*Active Site Structures.* Figures 4, 5, and 7 detail the marked similarities between CCP and the APX monomer overall and in the proximal/distal sides of the heme. His42 (analogous to CCP His52) and Arg38 (analogous to CCP Arg48) share identical conformations on the distal heme side. APX Trp41 is also present on the distal heme side in the same conformation as CCP Trp51. Also, Figure 4 indicates that the qualitative exposure of the distal heme plane is similar in the APX monomer and in CCP. More importantly, in the APX proximal heme side, Asp208, proximal ligand His163, and Trp179 are in conformations nearly identical to those in CCP for Asp235, His175, and Trp191. Trp191 in CCP is the amino acid residue that forms a stable, cation free radical that stores one of two oxidizing equivalents when CCP reacts with $H_2O_2$ to form compound I (Sivaraja et al., 1989). APX is, now, the first example of a plant peroxidase that contains a proximal side Trp in the same conformation as Trp191 in CCP. Our preliminary UV−vis spectrophotometry indicated that APX forms an oxyferryl center and a porphyrin $\pi$ cation radical upon reaction with 1 molar equivalent of $H_2O_2$ (Patterson & Poulos, 1994). However, diagnosis of the presence or absence of a CCP-like Trp radical required a more sensitive spectroscopic method. The accompanying paper (Patterson et al., 1995) describes electron paramagnetic resonance (EPR) comparisons of the compound I spectra of APX and CCP that clearly indicate that APX does not form a CCP-like Trp radical, but instead a porphyrin $\pi$ cation radical. The crystal structure of APX demonstrates that the APX Trp179 is in exactly the same conformation as CCP Trp191, so that the relevant comparative question is as follows: What are the significant structural differences, if any, that lead to a Trp radical in CCP and a porphyrin radical in APX?

Recently, Goodin and McRee (1993) demonstrated, by site-directed mutagenesis at the CCP Asp235 position, that subtle changes in H-bond geometry influence CCP's reduction potential, anisotropy of the Trp191 radical, activity, and strength of the iron ligand field. The APX geometry of hydrogen bonds between Asp208, His163, and Trp179 mimics the geometry of the analogous residues in CCP. The average hydrogen bond distance from the four APX monomers for the Asp208−Trp179 H-bond was identical to that from CCP (2.8 Å for APX vs 2.8 Å for CCP); the average Asp208−His163 H-bond for the four monomers was slightly longer than the equivalent H-bond in CCP (3.2 Å for APX vs 3.0 Å for CCP). Therefore, the Asp−His hydrogen bond may be shorter in CCP, although this difference is near the edge of the error estimate and may or may not be significant. Nevertheless, the microenvironment near the His-Asp-Trp catalytic triad, such as neighboring amino acid side chains and solvent structure, is different in the two peroxidases, which could contribute to the relative stability of a Trp radical.

The most obvious difference between the two peroxidases that could contribute to the location of the compound I radical is the presence of a cation ~8.0 Å from the proximal Trp179 in APX. This cation site also is very similar to the proximal $Ca^{2+}$ sites located in fungal peroxidases (Poulos et al., 1992; Kunishima et al., 1994; Peterson et al., 1994; Sundaramoorthy et al., 1995), with the exception that in APX only one carboxylate group serves as a ligand, while in the fungal peroxidases, two carboxylates participate (see Results). The dielectric milieu between the cation and Trp179 is not completely solvent-free. Figure 9 shows the location of a water oxygen atom surrounded by two backbone amide atoms, one of which is the NH of Trp179, a Thr180 O$\gamma$1 atom, and three backbone carbonyl oxygen atoms that are within 3.5 Å of the water oxygen atom. A water molecule was also modeled, in this particular location, in LiP, ARP, and MnP (Poulos et al., 1993; Kunishima et al., 1994; Peterson et al., 1994; Sundaramoorthy et al., 1995). In APX, this water molecule is part of a direct, nonbonded connection between the Trp179 and the cation (Figure 9). Such an interaction would be expected to destabilize a positive charge on Trp179 and, hence, increase the redox potential of Trp179 relative to Trp191 in CCP. Our current working hypothesis is that the cation in APX is one of possibly several factors that make it more difficult to oxidize Trp179 than the corresponding Trp in CCP, and, therefore, APX forms a porphyrin $\pi$ cation radical in compound I rather than a Trp radical.

## ACKNOWLEDGMENT

The authors gratefully acknowledge the assistance of Drs. N.-H. Xuong and N. Narayana for providing access to and data collection services for the Mark III Area Detectors at the University of California at San Diego. W.R.P. thanks Dr. Hui-ying Li for crystallographic advice and Dr. D. J. Schuller for essential help with noncrystallographic averaging.

## REFERENCES

Brunger, A. T. (1992) *X-PLOR Version 3.1: A System for X-Ray Crystallography and NMR*, Yale University Press, New Haven, CT.

CCP4 (Collaborative Computing Project #4) (1994) *Acta Crystallogr. D50*, 760−763.

Chen, X., & Asada, K. (1989) *Plant Cell Physiol. 30*, 987−998.

Cowtan, K. D., & Main, P. (1993) *Acta Crystallogr. D49*, 148−157.

Dolphin, D., Forman, A., Borg, D. C., Fajer, J., & Felton, R. H. (1971) *Proc. Natl. Acad. Sci. U.S.A. 68*, 614−618.

Elia, M. R., Borraccino, G., & Dipierro, S. (1992) *Plant Sci. 85*, 17−21.

Evans, S. V. (1993) *J. Mol. Graph. 11*, 134−138.

Finzel, B. C., Poulos, T. L., & Kraut, J. (1984) *J. Biol. Chem. 259*, 13027−13036.

Fishel, L. A., Villafranca, J. E., Mauro, M. J., & Kraut, J. (1987) *Biochemistry 26*, 351−360.

Fitzgerald, P. M. D. (1988) *J. Appl. Crystallogr. 21*, 273−278.

Furey,W., & Swaminathan, S. (1990) 14th American Crystallography Assoc. Meeting, New Orleans, Abstr. PA33.

Glusker, J. P. (1991) *Adv. Protein Chem. 42*, 1−76.

Goodin, D. B., & McRee, D. E. (1993) *Biochemistry 32*, 3313−3324.

Honzatko, R. B. (1986) *Acta Crystallogr. A42*, 172−178.

Howard, A. J., Nielson, C., & Xuong, N. H. (1985) *Methods Enzymol. 114*, 452−471.

Howard, A. J., Gilliland, G. L., Finzel, B. C., Poulos, T. L., Ohlendorf, D. H., & Salemme, F. R. (1987) *J. Appl. Crystallogr. 20*, 383−387.

Jones, T. A. (1985) *Methods Enzymol. 115*, 157−171.

Koshiba, T. (1993) *Plant Cell Physiol. 34*, 713−721.

Kraulis, P. (1991) *J. Appl. Crystallogr. 24*, 946−950.

Kunishima, N., Fukuyama, K., Matsubara, H., Hatanaka, H., Shibano, Y., & Amachi, T. (1994) *J. Mol. Biol. 235*, 331−344

Luzzati, P. V. (1952) *Acta Crystallogr. 5*, 802−810.

Mauro, M. J., Fishel, L. A., Hazzard, J. T., Meyer, T. E., Tollin, G., Cusanovich, M. A., & Kraut, J. (1988) *Biochemistry 27*, 6243−6256.
McRee, D. E. (1992) *J. Mol. Graph. 10*, 44−47.
Mittler, R., & Zilinskas, B. (1991a) *Plant Physiol. 97*, 962−968.
Mittler, R., & Zilinskas, B. (1991b) *FEBS 289*, 257−259.
Nakano, Y., & Asada, K. (1981) *Plant Cell Physiol. 22*, 867−880.
Patterson, W. R., & Poulos, T. L. (1994) *J. Biol. Chem. 269*, 17020−17024.
Patterson, W. R., Poulos, T. L., & Goodin, D. B. (1995) *Biochemistry 34*, 4342−4345.
Pelletier, H., & Kraut, J. (1992) *Science 258*, 1748−1755.
Peterson, J. F. W., Kaziola, A., & Larsen, S. (1994) *FEBS Lett. 339*, 291−296.
Poulos, T. L., & Fenna, R. E. (1994) in *Metal Ions in Biological Systems* (Sigel, H., Ed.) pp 25−75, Marcel Dekker, Inc., New York.
Poulos, T. L., Edwards, S. L., Wariishi, H., & Gold, M. H. (1993) *J. Biol. Chem. 268*, 4429−4440.
Ramakrishnan, C., & Ramachandran, G. N. (1965) *Biophys. J. 5*, 909−933.
Richardson, J. S., & Richardson, D. C. (1989) in *Prediction of Protein Structure & the Principles of Protein Conformation* (Fasman, G. D., Ed.) pp 2−97, Plenum Press, New York.
Sivaraja, M., Goodin, D. B., Smith, M., & Hoffman, B. M. (1989) *Science 245*, 738−740.
Srinivasan, A. (1966) *Acta Crystallogr. 20*, 143.
Sundaramoorthy, M., Katsuyuki, K., Gold, M. H., & Poulos, T. L. (1995) *J. Biol. Chem.* (in press).
Toney, M. D., Hohenester, E., Cowan, S. W., & Jansonius, J. N. (1993) *Science 261*, 756−759.
Welinder, K. G. (1992) *Curr. Opin. Struct. Biol. 2*, 388−393.
Xuong, N. H., Nielson, C., Hamlin, R., & Anderson, D. (1985) *J. Appl. Crystallogr. 18*, 342−350.
Zhang, K. Y. J. (1993) *Acta Crystallogr. D49*, 213−222.

BI942625D